Temperature dependent characteristics of 980 nm two-dimensional bottom emitting VCSEL arrays

Te Li (李 特)[1,2], Yongqiang Ning (宁永强)[1], Yanfang Sun (孙艳芳)[1,2], Jinjiang Cui (崔锦江)[1,2], Li Qin (秦 莉)[1], Changling Yan (晏长岭)[3], Yan Zhang (张 岩)[1,2], Biao Peng (彭 彪)[1,2], Guangyu Liu (刘光裕)[1,2], Yun Liu (刘 云)[1], and Lijun Wang (王立军)[1]

[1]*State Key Laboratory of Excited State Processes, Changchun Institute of Optics, Fine Mechanics and Physics, Chinese Academy of Sciences, Changchun 130033*

[2]*Graduate School of the Chinese Academy of Sciences, Beijing 100039*

[3]*Changchun University of Science and Technology, Changchun 130021*

High power bottom-emitting $In_{0.2}Ga_{0.8}As/GaAs$ 4×4 two-dimensional vertical-cavity surface-emitting laser (VCSEL) arrays, with high output power in the 980-nm wavelength regime are reported. At room temperature, the 16-element array with 200-μm aperture size of individual elements shows a continuous wave output power of 1.21 W with a lasing wavelength of 981.9 nm. Temperature dependent characteristics of VCSEL arrays with 90-μm aperture size of individual elements are investigated. The lasing wavelength, optical output power and threshold current are measured at various heatsink temperatures. With the increase of heatsink temperature, the maximum output power and slope efficiency are greatly decreased. A red shift of lasing wavelength and a widening of the lasing spectrum are also observed.

OCIS codes: 250.7260, 140.3290, 120.6780.

Vertical-cavity surface-emitting lasers (VCSELs) are one of the most active areas in optoelectronics nowadays. They are widely applied in optical communication, optical interconnection, optical stage, and so on[1,2]. At the same time, VCSELs also have considerable potential for high power emission. With the growing market for high power semiconductor lasers in medicine, material treatment, free space communication, and laser pumping, it seems worthwhile of exploring the potential of VCSELs for medium or high power application[3,4]. To increase the overall optical output power, the total lasing area of VCSEL has to be enlarged. This can be done by increase of the active area of single devices or arranging device in two-dimensional arrays[5−8]. The temperature dependence of VCSELs has been an important issue in their development. But the temperature dependent relations of VCSEL arrays have not been investigated. The experiments within this paper, aim to show the relationship between the mechanisms governing the temperature dependence of the cavity and the active region of VCSELs.

The reflectivities of distributed Bragg reflector (DBR) in VCSELs are strongly wavelength dependent, leading to a sharp cavity resonance at the designed emission wavelength. Joule heating and poor dissipation of heat increase the temperature of the device. With the temperature increase, the cavity resonance and the gain spectrum shift to longer wavelengths at different rates, resulting of increase in the threshold current and a rollover in the emitted power.

Figure 1 illustrates the general configuration of selectively oxidized VCSELs. The multilayer wafer is grown by metal organic chemical vapor deposition on n-GaAs substrate. For emission wavelengths in the 980-nm spectral region, the inner cavity contains three 8-nm-thick $In_{0.2}Ga_{0.8}As$ quantum wells embedded in 10-nm-thick GaAs barriers. Quarter-wavelength $Al_xGa_{1-x}As$ cladding layers are introduced on both sides of the active region to improve longitudinal carrier confinement and make the inner region one wavelength thick. Top and bottom mirrors contain $Al_{0.9}Ga_{0.1}As/GaAs$ quarter-wavelength Bragg stacks. Single-step grading with 5-nm-thick layers of intermediate bandgap energy is used to reduce the electrical series resistance. Current is supplied through the carbon p-doped top and silicon n-doped bottom reflectors, where modulation is required for high performance devices. Current confinement is achieved by means of selective lateral oxidation of an extra AlAs layer about 30 nm thick placed directly above the top cladding layer. Oxidation is done in a 420 °C hot water vapor atmosphere, leading to lateral oxidation rates in the 1 μm/min. After oxidation, the surface is passivated with Al_2O_3 and a circular window on top of the mesa is opened to evaporate a full size p-type contact consisting of Ti-Au-Pt-Au to provide a homogeneous current distribution and serve as a metal pad for soldering. The contact is annealed and thick gold is plated over the pillar to facilitate heat-sinking and future bonding. The GaAs substrate is mechanically thinned and chemically polished down to about 180 μm to decrease the substrate contribution to series resistance, and an antireflection

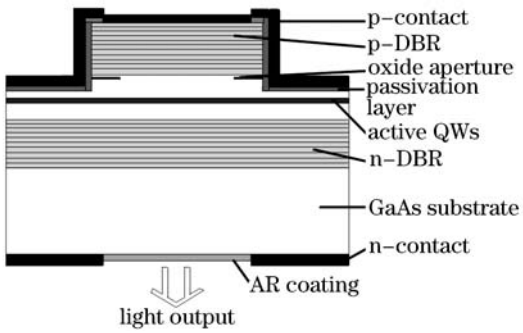

Fig. 1. Schematic layer structure of an individual element in array.

coating of HfO_2 with quarter-wavelength thickness is deposited on the polished substrate. Ge-Au-Ni-Au is evaporated around the HfO_2 window to form the large-area electrical contact. The whole chip is annealed at 380 °C in nitrogen environment condition for 60 s. Finally, the device is simply soldered upon a small copper heat sink with indium solder.

The VCSEL arrays with 200-μm aperture size of individual elements operate in continuous wave (CW) condition at room temperature (24 °C). Figure 2 shows its light power-current (P-I) characteristics. Threshold current of the device is about 1.32 A. The maximum CW optical output power is up to 1.21 W at a current of 6 A. The inset in Fig. 2 shows the lasing spectrum at a current of 6 A. The peak wavelength is 981.9 nm and the full-width at half-maximum (FWHM) of the spectrum is 0.7 nm.

The P-I characteristics at various heatsink temperatures of the VCSEL arrays with a active region diameter of the individual element of 90 μm are shown in Fig. 3. The device exhibits a threshold current of 0.52 A, a slop efficiency of about 0.25 W/A and a maximum output power of approximate 0.45 W at 20 °C. On the other hand, when the heatsink temperature is raised to 90 °C, the output power and slop efficiency decrease to 0.18 W and 0.09 W/A, respectively. In other words, a drastic reduction of output power and slop efficiency occurs with increasing temperature. The reduction of output power with temperature can be interpreted as the degradation of the InGaAs active region and the increased gain-cavity detuning. At the same time, it is observed that the rollover of output power is more serious when the heatsink temperature is raised.

The variation of lasing threshold current with temperature is shown in Fig. 4. The temperature varies from 20 to 90 °C. The lowest threshold current is observed between 40 and 50 °C. The threshold current decreases monotonically with increasing heatsink temperature in the low temperature range from 20 to 40 °C due to the negative gain-cavity offset and increases in the high temperature range from 50 to 90 °C due to the positive gain-cavity offset. This is a typical temperature dependence of the threshold current due to the gain-cavity offset in the VCSEL structure.

At the same time, the lasing spectrum characteristics with varying temperature are also measured. Figure 5 shows the lasing spectra of the VCSEL arrays under CW operation. The lasing peak wavelength is 993.5 nm with

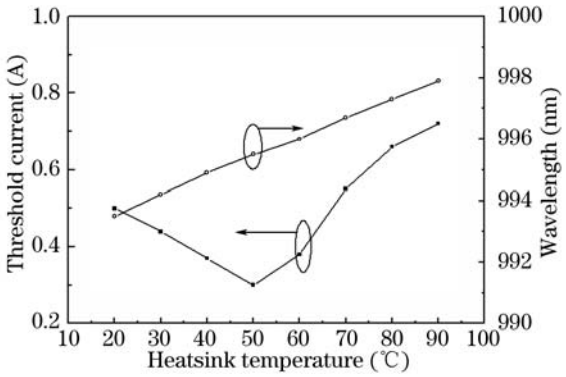

Fig. 4. Threshold current and wavelength shift of the device at different heatsink temperatures.

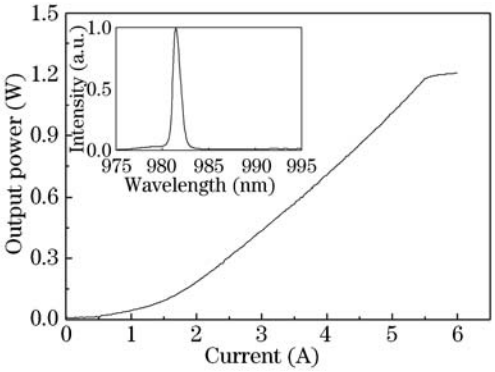

Fig. 2. Output power-current curves for a VCSEL array.

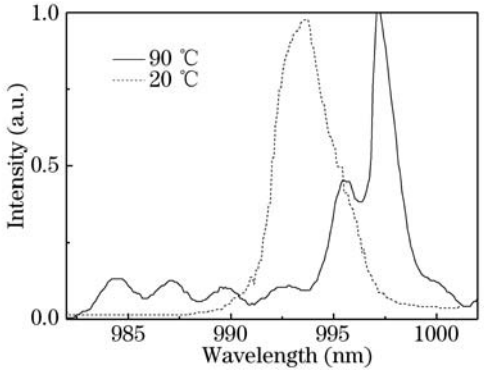

Fig. 5. Lasing spectra of the device at 20 and 90 °C.

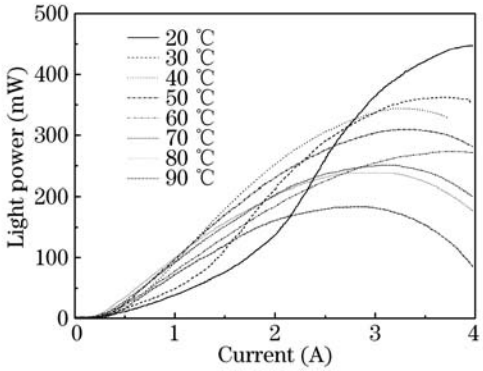

Fig. 3. Output power-current curves for array at various heatsink temperatures.

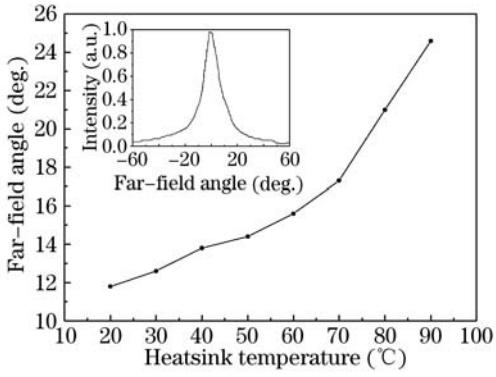

Fig. 6. Temperature dependence of far-field angle.

a FWHM of 2.9 nm at 20 °C. When the temperature is raised to 90 °C, the lasing peak wavelength moves to 997.9 nm and some side-lobes appear in the spectra. The wavelength redshift is 4.4 nm, which is given by the cavity resonance, leading to a shift of 0.06 nm/°C. More detail of lasing wavelength is plotted in Fig. 4.

The inset in Fig. 6 shows the far-field patterns at a current of 4 A and a temperature of 30 °C. Unlike the far-field ring-shaped beam profile, a more homogeneous current density distribution across the active area results in a high-quality output beam. But, the far-field patterns are also affected by the heatsink temperature. Figure 6 shows the change of far-field angle of the array for temperature between 20 and 90 °C. It is apparent that the beam quality of device is deteriorated when the temperature is raised. The influence of carriers distribution might be responsible for this effect, but further investigations are required for clarification.

In conclusion, the fabrication of bottom-emitting InGaAs VCSEL arrays is reported. The array consisting of 16 elements with an individual active diameter of 200 μm shows an output powers of 1.21 W. The temperature dependent characteristics of the arrays, which consist of 16 elements with an individual active diameter of 90 μm are investigated. A drastic reduction of output power and slop efficiency is observed with increasing temperature. When the heatsink temperature is 50 °C, the minimum threshold current is observed. The wavelength shift and far-field patterns of the device with temperature are also studied, and the wavelength shift with temperature is about 0.06 nm/°C.

This work was supported by the National Natural Science Foundation of China under Grant. No. 60636020, 60676034, 60577003. T. Li's e-mail address is lite810622@sohu.com.

References

1. R. Jäger, M. Grabherr, C. Jung, R. Michalzik, G. Reiner, B Weigl, and K. J. Ebeling, Electron. Lett. **33,** 330 (1997).
2. M. C. Amann, M. Ortsiefer, R. Shau, and J. Robkopf, Proc. SPIE **4871,** 123 (2002).
3. Y. Ma, C. Wang, and T. Miao, Optics and Precision Engineering (in Chinese) **13,** 253 (2005).
4. P. Lan, Y. chen, K. Huang, H. Lai, and J. Pan, IEEE Photon. Technol. Lett. **14,** 272 (2002).
5. M. Grabherr, B. Weigl, G. Reiner, R. Michalzik, M. Miller, and K. J. Ebeling, Electron. Lett. **32,** 1723 (1996).
6. M. Miller, M. Grabherr, R. King, R. Jäger, R. Michalzik, and K. J. Ebeling, IEEE J. Sel. Top. Quantum Electron. **7,** 210 (2001).
7. L. A. D'Asaro, J.-F. Seurin, and J. D. Wynn, Photonics Spectra **39,** 64 (2005).
8. T. Li, Y. Ning, Y. Sun, Z. Jin, Y. Liu, and L. Wang, Proc. SPIE **6028,** 602816 (2006).